ACADEMIC PRESS

Available online at www.sciencedirect.com

SCIENCE DIRECT®

Journal of Sound and Vibration 263 (2003) 643–663

JOURNAL OF SOUND AND VIBRATION

www.elsevier.com/locate/jsvi

Analysis of a disk-type stator for the piezoelectric ultrasonic motor using impedance matrix

Young H. Kim[a], Sung K. Ha[b,*]

[a] *Digital Appliance Research Laboratory, LG electronics, 327-23 Gasan-dong, Keumchun-gu, Seoul 153-802, South Korea*
[b] *Smart Structures and Materials Laboratory, Department of Mechanical Engineering, Hanyang University, 1271 Sa1-Dong, Ansan, Kyounggi-do 425-791, South Korea*

Received 15 November 2001; accepted 8 July 2002

Abstract

Impedance and admittance matrices of a piezoelectric annular actuator with segmented electrodes are presented for the analysis of the disk-type piezoelectric ultrasonic motors (USM). Equations of motion and the conjugate parameters for the impedance and admittance matrices are derived using the variational principle. In the derivation, the electric field in the piezoelectric layer is assumed to be constant over the area covered by a particular electrode, and the effects of both shear deformation and rotary inertia are taken into account. The resonance and antiresonance frequencies and the vibrating modes are calculated for the various resonance modes and boundary conditions, and the results are compared with those by the three-dimensional finite element methods. They are in excellent agreement with each other. It is expected that the derived impedance matrix can be effectively applied to the analysis and the design of the USM.

1. Introduction

Ultrasonic motors (USM), compared to conventional electromagnetic motors, have high stall torque, output torque at low speed, simple construction, and high resolution of displacement control. For this reason, USM are suitable to special applications such as auto-focus camera lenses, actuators for robots and rovers, watch motors, etc. [1–5]. To generate output torque, USM use two energy conversions: electrical energy from the power supply generates the elliptic motion on the stator surface by the piezoelectric effect, then the microscopic vibration of the stator is converted to the macroscopic motion of the rotor by the friction between the stator and the rotor. Piezoelectric annular actuators with segmented electrodes are used in the disk-type traveling wave USM to generate elliptic motion on the stator surface. Generally, the piezoelectric motor stators

*Corresponding author. 101 Alma Street Apt. 104, Palo Alto, CA 94301. USA..
E-mail address: sungha@stanford.edu, sungha@hanyang.ac.kr (S.K. Ha).

0022-460X/03/$ - see front matter
PII: S0022-460X(02)01107-0

are designed to operate at the resonance frequency above 20 kHz where shear deformation and rotary inertia have significant effects on the vibration characteristics of the stator.

After the traveling wave USM was first developed by Sashida [6] and industrially produced by Canon for auto-focus lenses [4], many investigations were made into the dynamic behavior of the traveling wave USM. Yamabuchi and Kagawa [7] and Maeno et al. [8] calculated the vibration mode of the ring-type stator and simulated dynamic response of piezoelectric motors using the three-dimensional finite element method (FEM), and the analysis is extended to the transient response [9]. Hagedorn et al. [10,11] presented mathematical model of the stator and investigated the effects of the rotary inertia on the vibration characteristics of the stator using finite difference method. FEM and finite difference method can take into account the detailed geometry of the stator and the effects of shear deformation and rotary inertia; however, they are computationally too expensive as a design tool. Hagood et al. [12] employed the Rayleigh–Ritz assumed mode energy method to model dynamic behavior of the stator, and Hagedorn et al. [13], based on the approach suggested by Hagood, simulated steady state dynamic behavior of the USM in the frequency domain considering the rotor flexibility. However, shear deformation and rotary inertia was not considered in the analysis. Using the thin plate theory, Friend et al. [14] calculated the dynamic behavior of the piezoelectric motor stator of constant thickness in the radial direction and predicted the resulting motion of the teeth. Hirose et al. proposed the usage of the antiresonance mode for USM because antiresonance state can provide the same mechanical vibration level with less heat generation [15–16]. The impedance matrices are often used in the analysis of the piezoelectric or non-piezoelectric structures since the lumped parameters conveniently describe the electromechanical behavior and make it easy to visualize the interactions of the compound structures with external systems, such as electrical driving devices and wave propagation medium [17–19].

In this paper, impedance and admittance matrices of the piezoelectric annular actuator with segmented electrodes in harmonic vibration are presented for the analysis of the disk-type piezoelectric motor stator. Motional equations and the conjugate parameters for the impedance and admittance matrices are derived using the variational principle, and both shear deformation and rotary inertia have been considered. The electromechanical responses of the piezoelectric actuator in harmonic vibration are calculated using the derived matrices, and the results are compared with those by the three-dimensional FEM.

2. Equations of motion and boundary conditions

The configuration of the piezoelectric annular actuator under consideration is shown in Fig. 1. The inner radius, the outer radius, and the thickness of the metal plate and the pth piezoelectric layer are denoted by r_a, r_b, h_s, and $h^{(p)}$, respectively; the superscript (p) denotes either a top layer (t) or a bottom layer (b). The piezoelectric actuator has segmented electrodes, which are driven in a repeating pattern: $\cos\omega t$, $\sin\omega t$, $-\cos\omega t$, $-\sin\omega t$, as shown in Fig. 1, and an electrode segment covers a quarter wavelength of the generated standing wave. A traveling wave is generated within the stator by the two temporally and spatially orthogonal standing waves that are excited by the electrode A and B, respectively. The stiffness of the electrode is neglected, and the actuator is considered as an annular plate in radial and circumferential flexural motion with constant thickness. A perfect bonding is assumed between the piezoelectric layer and the metal plate. Top

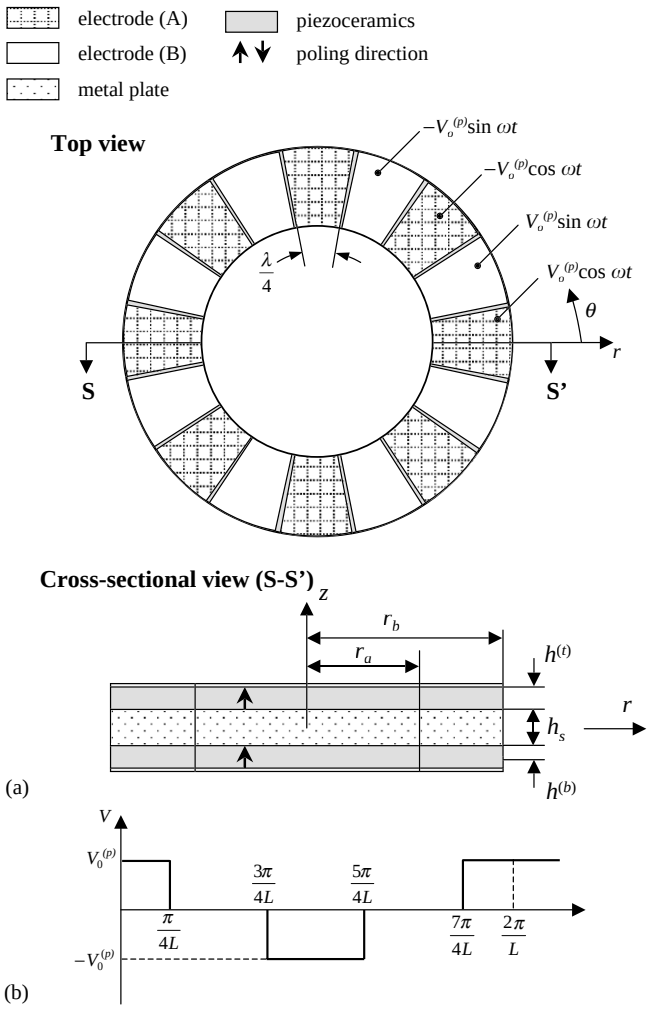

Fig. 1. (a) Configuration and electrode pattern of the piezoelectric actuator for $L-\lambda$ traveling wave excitation; $L=4$ and (b) the voltage applied at electrode A for a standing wave excitation.

and bottom piezoelectric layers are connected in parallel to generate the flexural motion of the stator. Neglecting the normal stress and strain components in the z direction and the r and θ directional electric fields, piezoelectric constituent equations for the point group 6 mm piezoceramics can be written as [2]

$$\begin{aligned} T_{rr} &= c_{11}S_{rr} + c_{12}S_{\theta\theta} - e_{31}E_z, \\ T_{\theta\theta} &= c_{12}S_{rr} + c_{22}S_{\theta\theta} - e_{31}E_z, \\ T_{\theta z} &= c_{44}S_{\theta z}, \\ T_{rz} &= c_{55}S_{rz}, \\ T_{r\theta} &= c_{66}S_{r\theta}, \\ D_z &= e_{31}(S_{rr} + S_{\theta\theta}) + \varepsilon_{33}E_z. \end{aligned} \tag{1}$$

The material properties in Eq. (1) have the following relationships:

$$c_{11} = c_{22} = \frac{1}{s_{11}^E(1-v^2)}, \quad c_{12} = vc_{11}, \quad c_{44} = c_{55} = c_{66} = \frac{1}{s_{44}^E},$$
$$e_{31} = \frac{d_{31}}{s_{11}^E(1-v)}, \quad \varepsilon_{33} = \varepsilon_{33}^{\mathrm{T}} - \frac{2d_{31}^2}{s_{11}^E(1-v)}. \tag{2}$$

T_{ij} and S_{ij} in Eq. (1) are the stress and strain components, D_z and E_z are the z directional electric displacement and field, respectively, c_{ij} and s_{ij}^E are the elastic stiffness and compliance under the constant electric field, d_{31} and e_{31} are the piezoelectric strain and stress constant; $\varepsilon_{33}^{\mathrm{T}}$ and ε_{33} are the dielectric constant under constant stress and constant strain, respectively, v denotes a planar Poisson ratio.

The steady state behavior of the piezoelectric actuator under harmonic excitation is considered here, therefore, the mechanical and electrical responses as well as the applied voltages and loads are supposed to be in harmonic motion with a common angular frequency ω and the time dependency of all the variables, which can be denoted by $e^{j\omega t}$, is omitted in the following analysis. The displacements, based on the first order shear deformation theory, are supposed to be

$$u_r(r,\theta,z) = -z\psi_r, \quad u_\theta(r,\theta,z) = -z\psi_\theta, \quad u_z(r,\theta,z) = u_z(r,\theta), \tag{3}$$

where the extensional motion of the neutral plane due to the asymmetry of the actuators in the thickness direction is neglected. In Eq. (3), ψ_r and ψ_θ are the rotation of the normal about the r- and θ-axis, respectively. Strain–displacement relationships can then be expressed as

$$S_{rr} = -z\psi_{r,r}, \quad S_{\theta\theta} = -\frac{z}{r}(\psi_r + \psi_{\theta,\theta}), \tag{4a}$$

$$S_{\theta z} = -\psi_\theta + \frac{1}{r}u_{z,\theta}, \quad S_{rz} = -\psi_r + u_{z,r}, \tag{4b}$$

$$S_{r\theta} = -\frac{z}{r}\psi_{r,\theta} + \frac{z}{r}\psi_\theta - z\psi_{\theta,r}. \tag{4c}$$

Assuming that the thickness of each piezoelectric layer is relatively thin compared with the total thickness of the actuator, the electric field is approximated to be constant through the thickness of the piezoelectric layer

$$E_z^{(p)}(\theta) = \frac{V^{(p)}(\theta)}{h^{(p)}}, \tag{5}$$

where $V^{(p)}(\theta)$ is the electric potential difference between the top and bottom electrode segments of the piezoelectric actuator and the function of the θ, as shown in Fig. 1(b). Internal energy W of the piezoelectric actuator in harmonic vibration with an angular frequency ω can be written as follows:

$$W = \frac{1}{2}\int\int_v\int \{-\rho\omega^2u_r^2 - \rho\omega^2u_\theta^2 - \rho\omega^2u_z^2 + T_{rr}S_{rr} + T_{\theta\theta}S_{\theta\theta} + T_{r\theta}S_{r\theta} + T_{rz}S_{rz} + T_{\theta z}S_{\theta z} - D_zE_z\}r\,\mathrm{d}r\,\mathrm{d}\theta\,\mathrm{d}z, \tag{6}$$

where υ denotes the total volume of the piezoelectric actuator and ρ is the mass density. Applying the variational principle yields

$$\begin{aligned}\delta W = &- \iint \{(rM_{rr})_{,r} - M_{\theta\theta} + M_{r\theta,\theta} + rR_{rz} + \rho_R\omega^2 r\psi_r\}\delta\psi_r \,\mathrm{d}r\,\mathrm{d}\theta \\ &- \iint \{M_{\theta\theta,\theta} + (rM_{r\theta})_{,r} + M_{r\theta} + rR_{\theta z} + \rho_R\omega^2 r\psi_\theta\}\delta\psi_\theta \,\mathrm{d}r\,\mathrm{d}\theta \\ &- \iint \{(rR_{rz})_{,r} + R_{\theta z,\theta} + \rho_h\omega^2 r u_z\}\delta u_z \,\mathrm{d}r\,\mathrm{d}\theta \\ &+ \int_0^{2\pi} rM_{rr}\delta\psi_r\Big|_{r_a}^{r_b}\mathrm{d}\theta + \int_0^{2\pi} rM_{r\theta}\delta\psi_\theta\Big|_{r_a}^{r_b}\mathrm{d}\theta + \int_0^{2\pi} rR_{rz}\delta u_z\Big|_{r_a}^{r_b}\mathrm{d}\theta \\ &- \frac{1}{h^{(t)}}\iiint_{(t)} rD_z^{(t)}\delta V^{(t)}\,\mathrm{d}r\,\mathrm{d}\theta\,\mathrm{d}z - \frac{1}{h^{(b)}}\iiint_{(b)} rD_z^{(b)}\delta V^{(b)}\,\mathrm{d}r\,\mathrm{d}\theta\,\mathrm{d}z, \end{aligned} \tag{7}$$

where ρ_h and ρ_R indicate the mass density and the rotary inertia per unit area. Moments M_{rr}, $M_{\theta\theta}$, $M_{r\theta}$ and shear forces R_{rz}, $R_{\theta z}$ in Eq. (7) are

$$\begin{pmatrix} M_{rr} \\ M_{\theta\theta} \\ M_{r\theta} \\ R_{rz} \\ R_{\theta z} \end{pmatrix} = \begin{bmatrix} D_{11} & D_{12} & 0 & 0 & 0 \\ D_{12} & D_{11} & 0 & 0 & 0 \\ 0 & 0 & D_{66} & 0 & 0 \\ 0 & 0 & 0 & G_{44} & 0 \\ 0 & 0 & 0 & 0 & G_{44} \end{bmatrix} \begin{pmatrix} \psi_{r,r} \\ (\psi_r + \psi_{\theta,\theta})/r \\ (\psi_{r,\theta} - \psi_\theta)/r + \psi_{\theta,r} \\ u_{z,r} - \psi_r \\ u_{z,\theta}/r - \psi_\theta \end{pmatrix} + \begin{pmatrix} M^*(\theta) \\ M^*(\theta) \\ 0 \\ 0 \\ 0 \end{pmatrix}, \tag{8}$$

where the equivalent flexural moment $M^*(\theta)$ due to the applied voltage is defined as

$$M^*(\theta) = \int e_{31}E_z z\,\mathrm{d}z = z_c^{(t)}e_{31}^{(t)}V^{(t)}(\theta) + z_c^{(b)}e_{31}^{(b)}V^{(b)}(\theta), \tag{9}$$

where $z_c^{(p)}$ denotes the z directional center co-ordinate of the pth piezoelectric layer with respect to the neutral axis, i.e., $z = 0$, which is determined from the condition

$$\int c_{11} z\,\mathrm{d}z = 0. \tag{10}$$

The state of the flexural moments and the shear forces are shown in Fig. 2. The stiffness G_{ij} and D_{ij} in Eq. (8) is defined as

$$(G_{ij}, D_{ij}) = \int (\kappa c_{ij}, c_{ij}z^2)\,\mathrm{d}z, \tag{11}$$

where κ is a shear correction factor ($\kappa = \pi^2/12$). Using Fourier series expansion, the rotations ψ_r, ψ_θ, the displacement u_z, and the applied voltage at the pth piezoelectric layer $V^{(p)}(\theta)$ can be expressed as follows:

$$\psi_r(r,\theta) = \sum_{m=1}^{\infty} \Psi_m^R(r)\cos m\theta, \tag{12a}$$

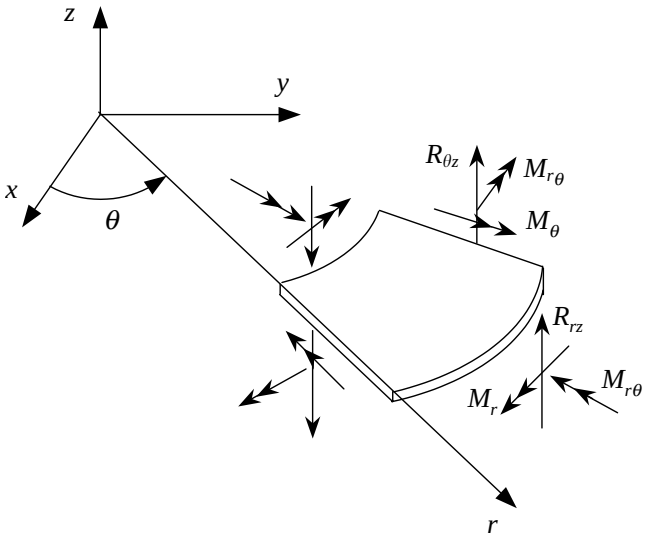

Fig. 2. The flexural moments M_{rr}, $M_{r\theta}$, M_{rr} and the shear force R_{rz}, $R_{\theta z}$ acting in the positive directions on the edges.

$$\psi_\theta(r,\theta) = \sum_{m=1}^{\infty} \Psi_m^{\Theta}(r) \sin m\theta, \tag{12b}$$

$$u_z(r,\theta) = \sum_{m=1}^{\infty} U_m(r) \cos m\theta, \tag{12c}$$

$$V^{(p)}(\theta) = V_0^{(p)} \sum_{m=1}^{\infty} \gamma_m \cos m\theta. \tag{12d}$$

For the applied voltage $V^{(p)}(\theta)$, as shown in Fig. 1, γ_m in Eq. (12d) can be determined as follows using the Fourier transform

$$\gamma_m = \frac{1}{\pi V_0^{(p)}} \int_0^{2\pi} V^{(p)}(\theta) \cos m\theta \, \mathrm{d}\theta = \begin{cases} \dfrac{4L}{m\pi} \sin \dfrac{m\pi}{4L}, & m = L, 3L, 5L, ..., \infty, \\ 0 & \text{otherwise}, \end{cases} \tag{13}$$

where L denotes the circumferential mode number of the traveling wave that the actuator is designed to excite. For other piezoelectric actuators, where a standing wave is generated by two electrode segments [12–14], γ_m becomes

$$\gamma_m = \begin{cases} \dfrac{4L_e}{m\pi} \sin \dfrac{m\pi}{2L}, & m = L, 3L, 5L, ..., \infty, \\ 0 & \text{otherwise}, \end{cases} \tag{14}$$

where L_e is $L/2-1$ or $L/2$ according to the existence or absence of the sensor. Using Eqs. (8), (9), (12) and (13), moments M_{rr}, $M_{\theta\theta}$, $M_{r\theta}$, and shear forces R_r, R_θ can be expressed as follows:

$$M_{rr}(r,\theta)=\sum_{m=0}^{\infty}M_m^{RR}(r)\cos m\theta, \tag{15a}$$

$$M_{\theta\theta}(r,\theta)=\sum_{m=0}^{\infty}M_m^{\Theta\Theta}(r)\cos m\theta, \tag{15b}$$

$$M_{r\theta}(r,\theta)=\sum_{m=0}^{\infty}M_m^{R\Theta}(r)\sin m\theta, \tag{15c}$$

$$R_{rz}(r,\theta)=\sum_{m=0}^{\infty}R_m^{RZ}(r)\cos m\theta, \tag{15d}$$

$$R_{\theta z}(r,\theta)=\sum_{m=0}^{\infty}R_m^{\Theta Z}(r)\sin m\theta, \tag{15e}$$

where

$$M_m^{RR}(r)=D_{11}\frac{\mathrm{d}\Psi_m^R(r)}{\mathrm{d}r}+D_{12}\frac{\Psi_m^R(r)+m\Psi_m^\Theta(r)}{r}+\gamma_m e_{31}^{(t)}z_c^{(t)}V_0^{(t)}+\gamma_m e_{31}^{(b)}z_c^{(b)}V_0^{(b)}, \tag{16a}$$

$$M_m^{\Theta\Theta}(r)=D_{12}\frac{\mathrm{d}\Psi_m^R(r)}{\mathrm{d}r}+D_{22}\frac{\Psi_m^R(r)+m\Psi_m^\Theta(r)}{r}+\gamma_m e_{31}^{(t)}z_c^{(t)}V_0^{(t)}+\gamma_m e_{31}^{(b)}z_c^{(b)}V_0^{(b)}, \tag{16b}$$

$$M_m^{R\Theta}(r)=D_{66}\left(-\frac{m\Psi_m^R(r)}{r}-\frac{\Psi_m^\Theta(r)}{r}+\frac{\mathrm{d}\Psi_m^\Theta(r)}{\mathrm{d}r}\right), \tag{16c}$$

$$R_m^{RZ}(r)=G_{44}\left(\frac{\mathrm{d}U_m(r)}{\mathrm{d}r}-\Psi_m^R(r)\right), \tag{16d}$$

$$R_m^{\Theta Z}(r)=G_{44}\left(-\frac{mU_m(r)}{r}-\Psi_m^\Theta(r)\right). \tag{16e}$$

Using Eqs. (1), (4), (12) and (13), and the orthogonality of the sine and cosine function, the last term in Eq. (7) can be expressed as follows:

$$\frac{1}{h^{(p)}}\int\int\int_{(p)}rD_z^{(p)}\delta V^{(p)}\mathrm{d}r\,\mathrm{d}\theta\,\mathrm{d}z=\left(\sum_{m=0}^{\infty}Q_m^{(p)}+C^{(p)}V_0^{(p)}\right)\delta V_0^{(p)}, \tag{17}$$

where $Q_m^{(p)}$ is the generated charge at the pth piezoelectric layer due to the displacement of mth circumferential mode and can be expressed as follows:

$$Q_m^{(p)} = \pi\gamma_m e_{31}^{(p)} z_c^{(p)} \left(r_a \Psi_m^R(r_a) - r_b \Psi_m^R(r_b) - m \int_{r_a}^{r_b} \Psi_m^\Theta(r)\,\mathrm{d}r \right). \tag{18}$$

In Eq. (17), $C^{(p)}$ is the clamped capacitance of the pth piezoelectric layer and defined as

$$C^{(p)} = \frac{\pi\varepsilon_{33}^{(p)}}{h^{(p)}} \frac{r_b^2 - r_a^2}{2}. \tag{19}$$

Using Eqs. (15) and (17), and the orthogonality of the sine and cosine function, Eq. (7) finally yields

$$\begin{aligned}\delta L = &\sum_{m=0}^{\infty} \pi r M_m^{RR}(r)\delta\Psi_m^R(r)\Big|_{r_a}^{r_b} + \sum_{m=0}^{\infty} \pi r M_m^{R\Theta}(r)\delta\Psi_m^\Theta(r)\Big|_{r_a}^{r_b} + \sum_{m=0}^{\infty} \pi r R_m^{RZ}(r)\delta U_m(r)\Big|_{r_a}^{r_b} \\ &- \left(\sum_{m=0}^{\infty} Q_m^{(t)} + C^{(t)} V_0^{(t)} \right) \delta V_0^{(t)} - \left(\sum_{m=0}^{\infty} Q_m^{(b)} + C^{(b)} V_0^{(b)} \right) \delta V_0^{(b)}\end{aligned} \tag{20}$$

with the flexural equilibrium equations for the mth circumferential mode

$$\frac{\mathrm{d}M_m^{RR}(r)}{\mathrm{d}r} + \frac{m}{r} M_m^{R\Theta}(r) + \frac{1}{r}(M_m^{RR}(r) - M_m^{\Theta\Theta}(r)) + R_m^{RZ}(r) + \rho_R \omega^2 \Psi_m^R(r) = 0, \tag{21a}$$

$$\frac{\mathrm{d}M_m^{R\Theta}(r)}{\mathrm{d}r} - \frac{m}{r} M_m^{\Theta\Theta}(r) + \frac{2}{r} M_m^{R\Theta}(r) + R_m^{\Theta Z}(r) + \rho_R \omega^2 \Psi_m^\Theta(r) = 0, \tag{21b}$$

$$\frac{\mathrm{d}R_m^{RZ}(r)}{\mathrm{d}r} + \frac{m}{r} R_m^{\Theta Z}(r) + \frac{R_m^{RZ}(r)}{r} + \rho_h \omega^2 U_m(r) = 0. \tag{21c}$$

If the displacement components $\Psi_m^R(r)$, $\Psi_m^\Theta(r)$ are expressed in terms of the potentials $\Phi_m(r)$ and $H_m(r)$ [20]

$$\Psi_m^R(r) = \frac{\mathrm{d}\Phi_m(r)}{\mathrm{d}r} + \frac{m}{r} H_m(r), \quad \Psi_m^\Theta(r) = -\frac{m}{r}\Phi_m(r) - \frac{\mathrm{d}H_m(r)}{\mathrm{d}r}, \tag{22}$$

and Eq. (16) is substituted into Eq. (21), the following coupled motional equations can be obtained:

$$\frac{\mathrm{d}}{\mathrm{d}r}\left(\nabla^2\Phi_m(r) - \frac{G_{44} - \rho_R\omega^2}{D_{11}}\Phi_m(r) + \frac{G_{44}}{D_{11}} U_m(r) \right) + \frac{1-\nu}{2}\frac{m}{r}(\nabla^2 - k^2) H_m(r) = 0, \tag{23a}$$

$$\left(\nabla^2\Phi_m(r) - \frac{G_{44} - \rho_R\omega^2}{D_{11}}\Phi_m(r) + \frac{G_{44}}{D_{11}} U_m(r) \right) + \frac{1-\nu}{2}\frac{r}{m}\frac{\mathrm{d}}{\mathrm{d}r}(\nabla^2 - k^2) H_m(r) = -\beta_m, \tag{23b}$$

$$\nabla^2 U_m(r) - \nabla^2 \Phi_m(r) + \frac{\rho_h \omega^2}{G_{44}} U_m(r) = 0, \tag{23c}$$

where the differential operator ∇^2 and the parameter k are defined as

$$\nabla^2 = \frac{\mathrm{d}}{\mathrm{d}r^2} + \frac{1}{r}\frac{\mathrm{d}}{\mathrm{d}r} - \frac{m^2}{r^2}, \quad k^2 = \frac{2}{1-v}\left(\frac{G_{44} - \rho_R \omega^2}{D_{11}}\right). \tag{24}$$

In Eq. (23), the parameter β_m is the function of applied voltage and can be written as follows:

$$\beta_m = \frac{\gamma_m}{D_{11}}(e_{31}^{(t)} z_c^{(t)} V_0^{(t)} + e_{31}^{(b)} z_c^{(b)} V_0^{(b)}). \tag{25}$$

Notice that the differential Eq. (23b) is non-homogeneous due to the applied voltages at the piezoelectric layer. $H_m(r)$ may be separated from $\Phi_m(r)$ and $U_m(r)$ by differentiation, addition, and subtraction of Eqs. (23a) and (23b):

$$\nabla^2(\nabla^2 - k^2) H_m(r) = 0, \tag{26a}$$

$$\nabla^2\left(\nabla^2 \Phi_m(r) - \frac{G_{44} - \rho_R \omega^2}{D_{11}} \Phi_m(r) + \frac{G_{44}}{D_{11}} U_m(r)\right) = \frac{m^2}{r^2} \beta_m. \tag{26b}$$

Using Eqs. (23b), (23c) and (26a), the potential Φ_m can be expressed in terms of U_m:

$$\Phi_m(r) = \frac{D_{11}}{G_{44} - \rho_R \omega^2}\left[\nabla^2 U_m(r) + \left(\frac{G_{44}}{D_{11}} + \frac{\rho_h \omega^2}{G_{44}}\right) U_m(r) + \beta_m\right]. \tag{27}$$

Then, decoupled differential equations for U_m and H_m can be obtained using Eqs. (26) and (27):

$$(\nabla^2 - k^2) H_m(r) = 0, \tag{28a}$$

$$(\nabla^2 + \lambda_1^2)(\nabla^2 - \lambda_2^2) U_m(r) = \frac{m^2}{r^2} \beta_m, \tag{28b}$$

where the parameters λ_1 and λ_2 are the functions of the angular frequency ω, each defined as

$$\lambda_1^2 = \frac{1}{2}\left(\frac{\rho_h \omega^2}{G_{44}} + \frac{\rho_R \omega^2}{D_{11}}\right) + \sqrt{\frac{1}{4}\left(\frac{\rho_R \omega^2}{D_{11}} - \frac{\rho_h \omega^2}{G_{44}}\right)^2 + \frac{\rho_h \omega^2}{D_{11}}}, \tag{29a}$$

$$\lambda_2^2 = -\frac{1}{2}\left(\frac{\rho_h \omega^2}{G_{44}} + \frac{\rho_R \omega^2}{D_{11}}\right) + \sqrt{\frac{1}{4}\left(\frac{\rho_R \omega^2}{D_{11}} - \frac{\rho_h \omega^2}{G_{44}}\right)^2 + \frac{\rho_h \omega^2}{D_{11}}}. \tag{29b}$$

The general solutions of Eq. (28) can be written as

$$H_m(r) = A_{1m} I_m(kr) + A_{2m} K_m(kr), \tag{30a}$$

$$U_m(r) = U_m^1(r) + U_m^2(r), \tag{30b}$$

where

$$U_m^1(r) = A_{3m}\mathrm{J}_m(\lambda_1 r) + A_{4m}\mathrm{Y}_m(\lambda_1 r) + \frac{\pi}{2}\frac{m^2\beta_m}{\lambda_1^2+\lambda_2^2}\big(\mathrm{J}_m(\lambda_1 r)\mathrm{Y}_m^{\mathrm{I}}(r) - \mathrm{Y}_m(\lambda_1 r)\mathrm{J}_m^{\mathrm{I}}(r)\big), \tag{31a}$$

$$U_m^2(r) = A_{5m}\mathrm{I}_m(\lambda_2 r) + A_{6m}\mathrm{K}_m(\lambda_2 r) + \frac{m^2\beta_m}{\lambda_1^2+\lambda_2^2}\big(\mathrm{I}_m(\lambda_2 r)\mathrm{K}_m^{\mathrm{I}}(r) - \mathrm{K}_m(\lambda_2 r)\mathrm{I}_m^{\mathrm{I}}(r)\big), \tag{31b}$$

where $\mathrm{J}_m(r)$ and $\mathrm{Y}_m(r)$ are the Bessel functions of the first and second kind of order m, respectively. $\mathrm{I}_m(r)$ and $\mathrm{K}_m(r)$ are the modified Bessel functions of the first and second kind of order m, respectively. In Eq. (31), the following abbreviations are used for notation brevity:

$$\begin{aligned} \mathrm{J}_m^{\mathrm{I}}(r) &= \int_{r_a}^{r} \mathrm{J}_m(\lambda_1 r)/r\,\mathrm{d}r, \quad \mathrm{Y}_m^{\mathrm{I}}(r) = \int_{r_a}^{r} \mathrm{Y}_m(\lambda_1 r)/r\,\mathrm{d}r \\ \mathrm{I}_m^{\mathrm{I}}(r) &= \int_{r_a}^{r} \mathrm{I}_m(\lambda_1 r)/r\,\mathrm{d}r, \quad \mathrm{K}_m^{\mathrm{I}}(r) = \int_{r_a}^{r} \mathrm{K}_m(\lambda_1 r)/r\,\mathrm{d}r. \end{aligned} \tag{32}$$

Using Eqs. (27), (28) and (30), the potential Φ_m in Eq. (27) can be rewritten as follows:

$$\Phi_m(r) = \alpha_1 U_m^1(r) + \alpha_2 U_m^2(r) + \frac{D_{11}}{G_{44} - \rho_R\omega^2}\beta_m, \tag{33}$$

where

$$\alpha_1 = 1 - \frac{D_{11}}{G_{44} - \rho_R\omega^2}\lambda_2^2, \quad \alpha_2 = 1 + \frac{D_{11}}{G_{44} - \rho_R\omega^2}\lambda_1^2. \tag{34}$$

when the applied voltages are zero, i.e., for the case of free vibration of the actuator under short circuit condition, and the actuator is a circular type, the coefficients A_{2m}, A_{4m}, A_{6m}, and β_m become zero and the results reduces to those presented by Mindlin et al. [21].

3. Impedance and admittance matrices

Near the resonance frequency, the displacements of the stator can be approximated as those of Lth circumferential vibrating mode. Therefore, the variations of the internal energy that is shown in Eq. (20) can be now approximated as follows:

$$\delta L \cong \mathbf{F}^{\mathrm{T}}\delta\mathbf{u} - \mathbf{Q}^{\mathrm{T}}\delta\mathbf{V}, \tag{35}$$

where each vector is defined as

$$\mathbf{F} = \begin{pmatrix} -\pi r_a M_L^{RR}(r_a) \\ -\pi r_a M_L^{R\Theta}(r_a) \\ -\pi r_a R_L^{RZ}(r_a) \\ \pi r_b M_L^{RR}(r_b) \\ \pi r_b M_L^{R\Theta}(r_b) \\ \pi r_b R_L^{RZ}(r_b) \end{pmatrix}, \quad \mathbf{u} = \begin{pmatrix} \Psi_L^R(r_a) \\ \Psi_L^{\Theta}(r_a) \\ U_L(r_a) \\ \Psi_L^R(r_b) \\ \Psi_L^{\Theta}(r_b) \\ U_L(r_b) \end{pmatrix}, \tag{36a}$$

$$\mathbf{Q} = \begin{pmatrix} Q^{(t)} \\ Q^{(b)} \end{pmatrix}, \quad \mathbf{V} = \begin{pmatrix} V_0^{(t)} \\ V_0^{(b)} \end{pmatrix}. \tag{36b}$$

Using Eqs. (16), (30) and (33), the force boundary conditions can be represented in a matrix form which is the function of displacements at the boundary and the voltages

$$\mathbf{F} = \mathbf{B}_h\mathbf{A} + \mathbf{B}_p\mathbf{V} + \mathbf{C}_E\mathbf{V}. \tag{37}$$

Similar to the force boundary conditions, the displacement boundary conditions can also be expressed in a matrix form by using Eqs. (30) and (33):

$$\mathbf{u} = \mathbf{G}_h\mathbf{A} + \mathbf{G}_p\mathbf{V}. \tag{38}$$

From Eq. (18), the charge vector can be expressed as follows:

$$\begin{aligned}\mathbf{Q} &= -\mathbf{C}_E\mathbf{u} + \mathbf{P}_h\mathbf{A} + \mathbf{P}_p\mathbf{V} + \mathbf{C}\mathbf{V} \\ &= -(\mathbf{C}_E - \mathbf{P}_h\mathbf{G}_h^{-1})\mathbf{u} + (\mathbf{C} + \mathbf{P}_p - \mathbf{P}_h\mathbf{G}_h^{-1}\mathbf{G}_p)\mathbf{V}.\end{aligned} \tag{39}$$

Eliminating the coefficient vector $\mathbf{A}$ from Eqs. (37) and (38) and using the symmetry of the matrix [22] that is manifested by the results of the variational analysis, i.e., Eq. (20), we obtain

$$\begin{pmatrix}\mathbf{F} \\ -\mathbf{Q}\end{pmatrix} = \begin{bmatrix}\mathbf{\Gamma}_M & \mathbf{\Gamma}_C^{\mathrm{T}} \\ sym. & -\mathbf{\Gamma}_E\end{bmatrix}\begin{pmatrix}\mathbf{u} \\ \mathbf{V}\end{pmatrix}, \tag{40}$$

where

$$\mathbf{\Gamma}_M = \mathbf{B}_h\mathbf{G}_h^{-1}, \tag{41a}$$

$$\mathbf{\Gamma}_C = \mathbf{C}_E - \mathbf{P}_h\mathbf{G}_h^{-1}, \tag{41b}$$

$$\mathbf{\Gamma}_E = \mathbf{C} + \mathbf{P}_p - \mathbf{P}_h\mathbf{G}_h^{-1}\mathbf{G}_p. \tag{41c}$$

The matrices $\mathbf{B}_h$, $\mathbf{G}_h$, $\mathbf{C}_E$, $\mathbf{P}_h$, $\mathbf{P}_p$, and $\boldsymbol{G}_{\mathrm{p}}$ in Eq. (41) are shown in Appendix A. Exchanging the charge vector for the voltage vector in Eq. (40) and employing generic velocity vector $\mathbf{U} = \mathrm{j}\omega\mathbf{u}$ and current vector $\mathbf{I} = \mathrm{j}\omega\mathbf{Q}$ easily yield the 8×8 impedance matrix $\mathbf{Z}$:

$$\begin{pmatrix}\mathbf{F} \\ \mathbf{V}\end{pmatrix} = \mathbf{Z}\begin{pmatrix}\mathbf{U} \\ \mathbf{I}\end{pmatrix}, \tag{42}$$

where

$$\mathbf{Z} = \frac{1}{\mathrm{j}\omega}\begin{bmatrix}\mathbf{\Gamma}_M + \mathbf{\Gamma}_C\mathbf{\Gamma}_E^{-1}\mathbf{\Gamma}_C^{\mathrm{T}} & \mathbf{\Gamma}_C\mathbf{\Gamma}_E^{-1} \\ sym. & \mathbf{\Gamma}_E^{-1}\end{bmatrix}. \tag{43}$$

The exchange of the force vectors for the velocity vectors in Eq. (40) yields the admittance matrix

$$\begin{pmatrix}\mathbf{U} \\ \mathbf{I}\end{pmatrix} = \mathrm{j}\omega\begin{bmatrix}\mathbf{\Gamma}_M^{-1} & \mathbf{\Gamma}_M^{-1}\mathbf{\Gamma}_C \\ sym. & \mathbf{\Gamma}_C^{\mathrm{T}}\mathbf{\Gamma}_M^{-1}\mathbf{\Gamma}_C + v_E\end{bmatrix}\begin{pmatrix}\mathbf{F} \\ \mathbf{V}\end{pmatrix}, \tag{44}$$

which enables us to calculate the mechanical and electrical responses of the piezoelectric transducers for the forces applied at the boundary and the voltages excited at the piezoelectric layers. The poles and zeros of electrical admittance in Eq. (44) give the characteristic equations, each for the resonance frequencies (RF) ω_r and the antiresonance frequencies (AF) ω_a of electric current. The amplitude of the vibration velocity and the currents near the resonance frequency can be calculated by employing mechanical, piezoelectric, and dielectric properties in complex forms [23]. In this case, the impedance

and admittance matrices become complex variables, but have the same form as those given in Eqs. (43) and (44). The derived impedance matrix in Eq. (43) is that of the closed annular actuator with constant thickness. For the piezoelectric motor stator that has radially stepwise varying thickness, the global impedance matrix can be obtained by combining the impedance matrices of each section according to the continuation conditions at the interfaces, i.e., at the inner and outer radii [24].

4. Results and discussion

In this section, the dynamic behavior of the piezoelectric annular actuator is investigated using the impedance and admittance matrices derived in the previous section. In the numerical calculations, PZT G1195N is used to actuate the motor stator and stainless steel is used for the metal plate. The material properties are as follows; for the G1195N, $1/s_{11}^E = 61.0\,\text{GPa}$, $\nu = 0.3$, $\rho = 7600.0\,\text{kg/m}^3$, $d_{31} = 0.254\,\text{nm/V}$, and $\varepsilon_{33}^{\text{T}} = 15.0\,\text{nF/m}$; for the stainless steel, $1/s_{11}^E = 200.0\,\text{GPa}$, $\nu = 0.3$, and $\rho = 7830.0\,\text{kg/m}^3$. The inner and outer radii of the actuator are 15.0 and 30.0 mm, respectively, and the thickness of the piezoelectric layer and the metal shim are 0.25 and 3.0 mm, respectively.

The RF and AF of the piezoelectric annular actuators are calculated for various boundary conditions and vibration mode. Three cases are investigated: (1) the effects of shear deformation and rotary inertia are neglected (no shear and no rotary inertia), (2) only the effect of rotary inertia is considered (only rotary inertia), and (3) the effects of shear deformation and rotary inertia are considered (both shear and rotary inertia). Three-dimensional FEM is used to verify the results by the present methods. The element has four degrees of freedom at a node, i.e., three mechanical displacements and one electric potential [25]. The sector of the stator which corresponds to a quarter wavelength is modelled by applying the symmetric and antisymmetric conditions at $\theta = 0$ and $\lambda/4$, respectively, that shows the same results as the full modelling of the annular actuator. The finite element model of the piezoelectric annular actuator is shown in

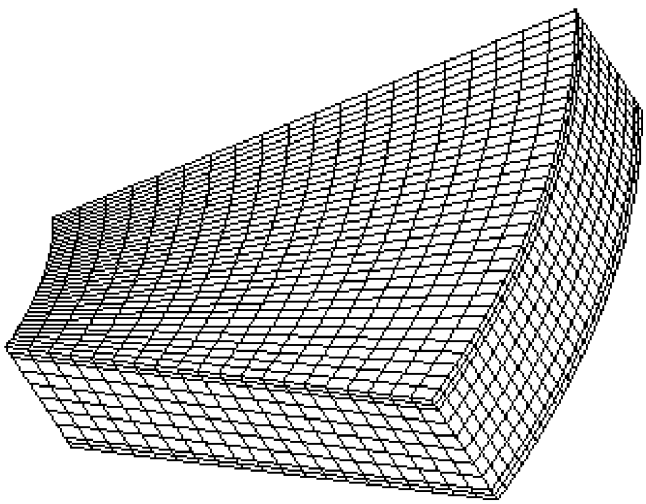

Fig. 3. FEM of the annular piezoelectric actuator.

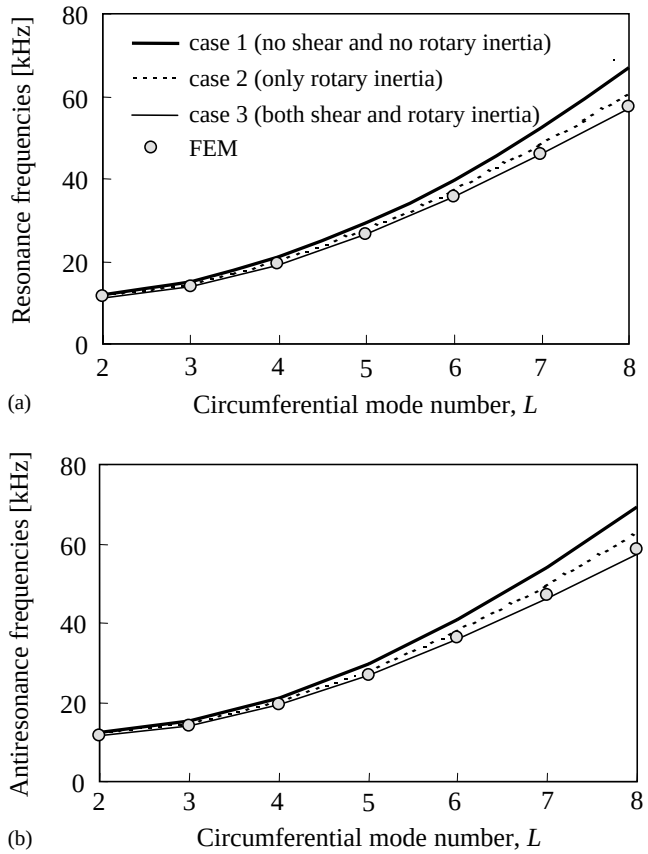

Fig. 4. (a) The RF and (b) the AF of the $(0, L)$ flexural mode versus the circumferential mode number L; the actuator is clamped at the inner radius and free at the outer radius.

Fig. 3. In the finite element analysis, the RF and the AF are calculated by the modal analysis under the conditions of short circuit and open circuit, respectively [26]. When the actuator is short-circuited, the electric field E_z in the piezoelectric layer becomes zero under the assumption of Eq. (5), and the stress–strain relations follow the non-piezoelectric constituent equations. In that case, the resonance occurs at the RF of the actuator. When the electrical port is opened ($I = 0$), the overall stiffness of the piezoelectric layer is increased, the resonance occurring at the AF of the actuator that is higher than the RF.

At first, the RF and the AF of $(0, L)$ mode of the actuator under clamped–free and free–free boundary conditions are calculated and shown in Figs. 4 and 5, respectively. The RF and the AF of case (3) are a little lower than those by the FEM with an error of 1%, which is caused by the assumption of constant electric field under each electrode segment. As the circumferential mode number L increases, the effects of rotary inertia and shear strain $S_{\theta z}$ increases, and the RF and the AF of case (1) and (2) have significant deviations from the results of the three-dimensional FEM, which shows the importance of rotary inertia and shear deformation for the lower ratio of the

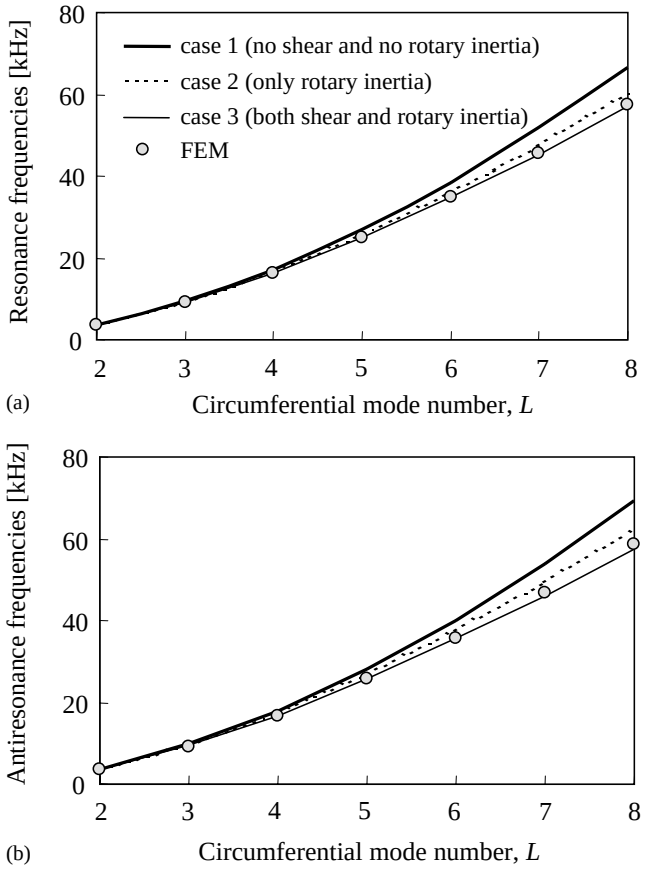

Fig. 5. (a) The RF and (b) the AF of the $(0, L)$ flexural mode versus the circumferential mode number L; the actuator is free at the inner and outer radii.

wavelength to the plate thickness. Overall, the differences of case (2) and (3) of the free–free boundary condition are less than those of the clamped–free boundary condition. It is because the shear deformation S_{rz} of the actuator under free-free boundary condition is less than those of the actuator under clamped–free boundary condition.

The RF and the AF of $(1, L)$ mode of the actuator under clamped–free and free–free boundary conditions are also shown in Figs. 6 and 7, respectively. As expected, the effects of shear deformation and the rotary inertia are higher than those of $(0, L)$ mode. The differences of case (2) and (3) when the boundary condition is clamped–free is insensitive to the circumferential mode number L because the differences are mainly due to shear deformation S_{rz} which is irrelative to L. However, for the free–free boundary condition, the difference of case (2) and (3) increases as the mode number increases because the differences mainly due to shear deformation $S_{\theta z}$. As the circumferential mode number increases, the effects of rotary inertia become more significant for the both boundary conditions because of the increase of resonance frequency. The RF and the AF calculated under the consideration of both shear and rotary inertia

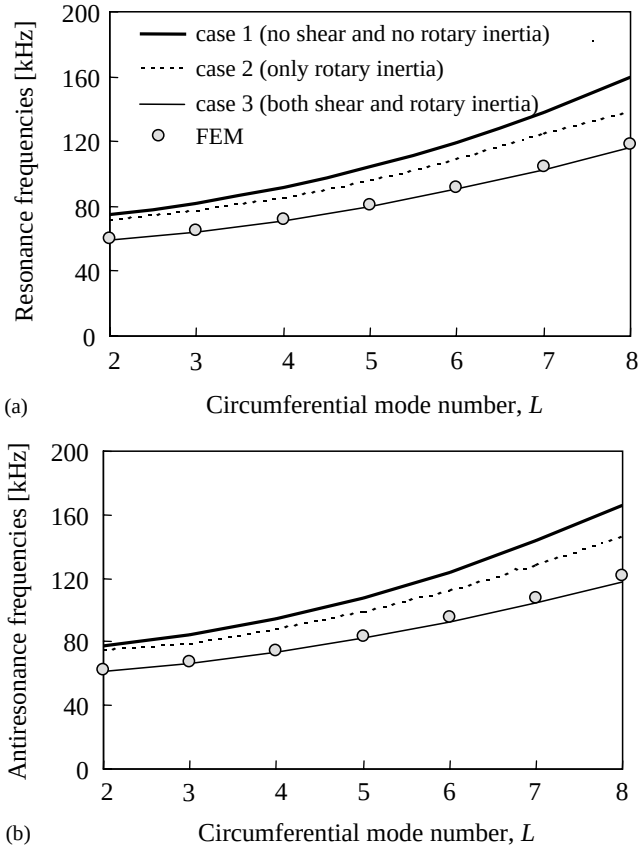

Fig. 6. (a) The RF and (b) the AF of the $(1, L)$ flexural mode versus the circumferential mode number L; the actuator is clamped at the inner radius and free at the outer radius.

agree very well with the results by the three-dimensional FEM for all ranges of circumferential mode number L.

The mode shapes for the short-circuit actuator under clamped–free and free–free boundary conditions, when the circumferential mode number L is 5, are calculated and shown in Figs. 8 and 9, respectively. The differences of mode shapes are not clearly shown when the radial mode number is 0, where the effects of shear deformation on the mode shape are small. However, when the radial mode number is 1, the differences of mode shapes are clearly shown, especially at the inner radius of clamped boundary condition, where the slope of transverse displacement is not zero for the case (3) and FEM because they allow shear deformation S_{rz}. This result in the difference of the position of zero slope where the tooth are mounted. If shear deformation is not considered, the position of zero slope, which is necessary in the design of $(1, L)$ mode disk-type USM [14,27], cannot be estimated accurately. It has been also observed that the vibrational mode shapes for the open-circuit condition show unnoticeable differences from those for the short-circuit condition while the AF are different from the RF.

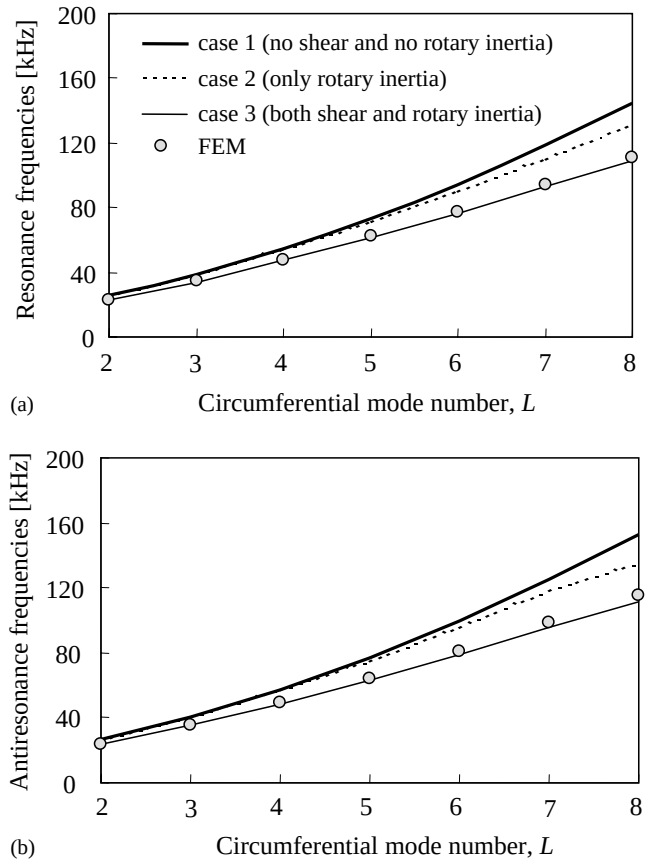

Fig. 7. (a) The RF and (b) the AF of the $(1, L)$ flexural mode versus the circumferential mode number L; the actuator is free at the inner and outer radii.

5. Conclusion

To analyze the dynamic behavior of disk-type USM, impedance and admittance matrices of the piezoelectric annular actuator with segmented electrodes are derived. In the derivation, the effects of both shear deformation and rotary inertia are considered. The dynamic behavior of the actuator is investigated using the derived matrices, and the results are compared with those by the three-dimensional FEM. The derived impedance and admittance matrices can be applied to the analysis of the disk-type USM with the stator/rotor interaction model, and the radially stepwise varying thickness of the stator can be taken into account by combining impedance matrices of each section according to the continuity condition. It is expected that the present method can be extended to the analysis of the beam or ring type ultrasonic motor.

Acknowledgements

This work was supported by the center for iDOT and the Brain Korea 21 Project.

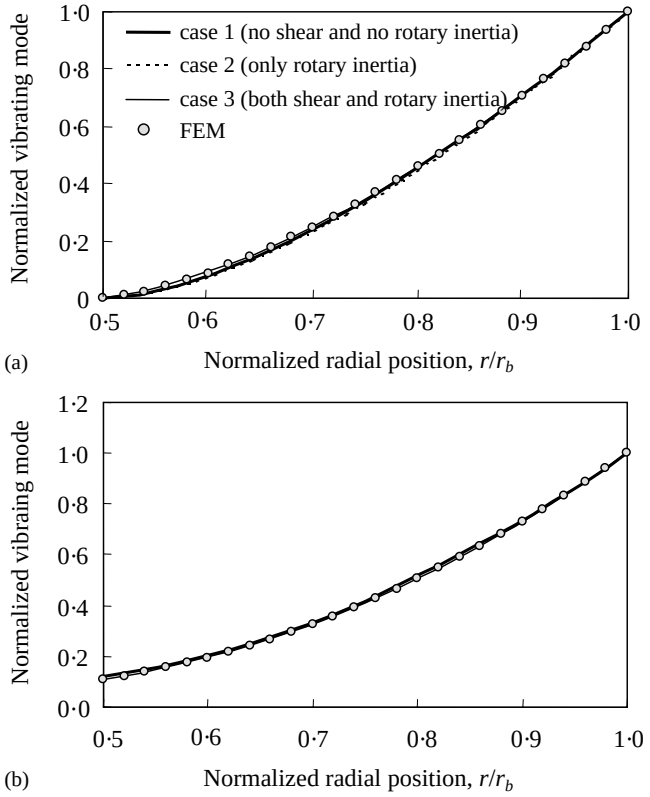

Fig. 8. Vibrating mode shape at the RF of (0, 5) flexural mode: (a) clamped–free boundary condition and (b) free–free boundary condition.

Appendix. A

All the components of the derived impedance matrix in Eq. (41) are presented. $\mathbf{G}_h$ and $\mathbf{B}_h$, which are the components the matrix Γ_M are as follows:

$$\mathbf{G}_h = \begin{pmatrix} \mathbf{G}_0|_{r=r_a} \\ \mathbf{G}_0|_{r=r_b} \end{pmatrix}, \quad \mathbf{B}_h = \begin{pmatrix} -\mathbf{B}_0|_{r=r_a} \\ \mathbf{B}_0|_{r=r_b} \end{pmatrix}, \tag{A.1}$$

where the matrices $\mathbf{G}_0$ and $\mathbf{B}_0$ are the functions of r and defined as

$$\mathbf{G}_0^{\mathrm{T}} = \begin{pmatrix} L\mathrm{I}_L(kr)/r & -\mathrm{I}_L^D(kr) & 0 \\ L\mathrm{K}_L(kr)/r & -\mathrm{K}_L^D(kr) & 0 \\ \alpha_1 \mathrm{J}_L^D(\lambda_1 r) & -\alpha_1 L\mathrm{J}_L(\lambda_1 r)/r & \alpha_1 \mathrm{J}_L(\lambda_1 r) \\ \alpha_1 \mathrm{Y}_L^D(\lambda_1 r) & -\alpha_1 L\mathrm{Y}_L(\lambda_1 r)/r & \alpha_1 \mathrm{Y}_L(\lambda_1 r) \\ \alpha_2 \mathrm{I}_L^D(\lambda_2 r) & -\alpha_2 L\mathrm{I}_L(\lambda_2 r)/r & \alpha_2 \mathrm{I}_L(\lambda_2 r) \\ \alpha_2 \mathrm{K}_L^D(\lambda_2 r) & -\alpha_2 L\mathrm{K}_L(\lambda_2 r)/r & \alpha_2 \mathrm{K}_L(\lambda_2 r) \end{pmatrix}, \tag{A.2a}$$

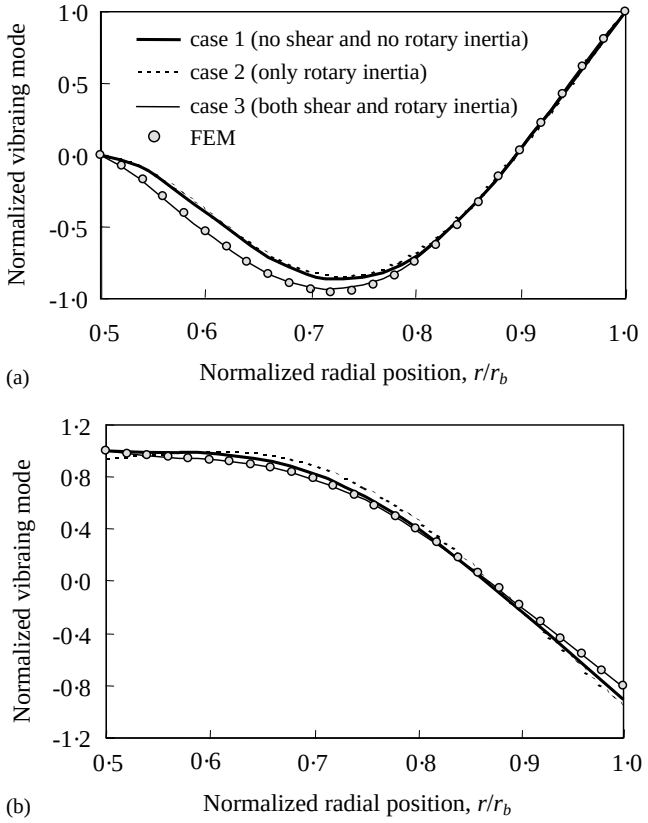

Fig. 9. Vibrating mode shape at the RF of (1, 5) flexural mode: (a) clamped–free boundary condition and (b) free–free boundary condition.

$$\mathbf{B}_0^{\mathrm{T}} = \begin{pmatrix} \sigma_1 \mathrm{I}_L(kr) + \sigma_2 \mathrm{I}_{L+1}(kr) & \sigma_7 \mathrm{I}_L(kr) + \sigma_8 \mathrm{I}_{L+1}(kr) & \sigma_{13} \mathrm{I}_L(kr) \\ \sigma_1 \mathrm{K}_L(kr) - \sigma_2 \mathrm{K}_{L+1}(kr) & \sigma_7 \mathrm{K}_L(kr) - \sigma_8 \mathrm{K}_{L+1}(kr) & \sigma_{13} \mathrm{K}_L(kr) \\ \sigma_3 \mathrm{J}_L(\lambda_1 r) + \sigma_4 \mathrm{J}_{L+1}(\lambda_1 r) & \sigma_9 \mathrm{J}_L(\lambda_1 r) + \sigma_{10} \mathrm{J}_{L+1}(\lambda_1 r) & \sigma_{14} \mathrm{J}_L^D(\lambda_1 r) \\ \sigma_3 \mathrm{Y}_L(\lambda_1 r) + \sigma_4 \mathrm{Y}_{L+1}(\lambda_1 r) & \sigma_9 \mathrm{Y}_L(\lambda_1 r) + \sigma_{10} \mathrm{Y}_{L+1}(\lambda_1 r) & \sigma_{14} \mathrm{Y}_L^D(\lambda_1 r) \\ \sigma_5 \mathrm{I}_L(\lambda_2 r) - \sigma_6 \mathrm{I}_{L+1}(\lambda_2 r) & \sigma_{11} \mathrm{I}_L(\lambda_2 r) - \sigma_{12} \mathrm{I}_{L+1}(\lambda_2 r) & \sigma_{15} \mathrm{I}_L^D(\lambda_2 r) \\ \sigma_5 \mathrm{K}_L(\lambda_2 r) + \sigma_6 \mathrm{K}_{L+1}(\lambda_2 r) & \sigma_{11} \mathrm{K}_L(\lambda_2 r) + \sigma_{12} \mathrm{K}_{L+1}(\lambda_2 r) & \sigma_{15} \mathrm{K}_L^D(\lambda_2 r) \end{pmatrix}, \tag{A.2b}$$

where the superscript D means the differentiation with respect to r, i.e.,

$$\mathrm{J}_L^D(\lambda_1 r) = \frac{\mathrm{d}\mathrm{J}_L(\lambda_1 r)}{\mathrm{d}r} = \frac{L\mathrm{J}_L(\lambda_1 r)}{r} - \lambda_1 \mathrm{J}_{L+1}(\lambda_1 r),$$
$$\mathrm{Y}_L^D(\lambda_1 r) = \frac{\mathrm{d}\mathrm{Y}_L(\lambda_1 r)}{\mathrm{d}r} = \frac{L\mathrm{Y}_L(\lambda_1 r)}{r} - \lambda_1 \mathrm{Y}_{L+1}(\lambda_1 r),$$

$$\mathrm{I}_L^D(\lambda_2 r) = \frac{\mathrm{d}\mathrm{I}_L(\lambda_2 r)}{\mathrm{d}r} = \frac{L\mathrm{I}_L(\lambda_2 r)}{r} + \lambda_2 \mathrm{I}_{L+1}(\lambda_2 r),$$
$$\mathrm{K}_L^D(\lambda_2 r) = \frac{\mathrm{d}\mathrm{K}_L(\lambda_2 r)}{\mathrm{d}r} = \frac{L\mathrm{K}_L(\lambda_2 r)}{r} - \lambda_2 \mathrm{K}_{L+1}(\lambda_2 r). \tag{A.3}$$

The parameters σ_i in Eq. (A.2b) are defined as follows for notation brevity:

$$\begin{aligned}
&\sigma_1 = \pi(L^2 - L)(D_{11} - D_{12})/r, && \sigma_2 = \pi Lk(D_{11} - D_{12}),\\
&\sigma_3 = \alpha_1(\sigma_1 - \pi D_{11}\lambda_1^2 r), && \sigma_4 = \pi\alpha_1\lambda_1(D_{11} - D_{12}),\\
&\sigma_5 = \alpha_2(\sigma_1 + \pi D_{11}\lambda_2^2 r), && \sigma_6 = \pi\alpha_2\lambda_2(D_{11} - D_{12}),\\
&\sigma_7 = \pi D_{66}(2L - 2L^2 - k^2 r^2)/r, && \sigma_8 = 2\pi k D_{66},\\
&\sigma_9 = 2\pi D_{66}\alpha_1(L - L^2)/r, && \sigma_{10} = 2\pi L D_{66}\alpha_1\lambda_1,\\
&\sigma_{11} = 2\pi D_{66}\alpha_2(L - L^2)/r, && \sigma_{12} = 2\pi L D_{66}\alpha_2\lambda_2,\\
&\sigma_{13} = -\pi L G_{44}, && \sigma_{14} = \pi G_{44}(1 - \alpha_1)r,\\
&\sigma_{15} = \pi G_{44}(1 - \alpha_2)r.
\end{aligned} \tag{A.4}$$

The matrices $\mathbf{C}_E$ and $\mathbf{P}$ of Eq. (41b) are as follows:

$$\mathbf{C}_E = \begin{pmatrix} -\pi\gamma_L z_c^{(t)} e_{31}^{(t)} r_a & 0 & 0 & \pi\gamma_L z_c^{(t)} e_{31}^{(t)} r_b & 0 & 0 \\ -\pi\gamma_L z_c^{(b)} e_{31}^{(b)} r_a & 0 & 0 & \pi\gamma_L z_c^{(b)} e_{31}^{(b)} r_b & 0 & 0 \end{pmatrix}, \tag{A.5a}$$

$$\mathbf{P}_h^{\mathrm{T}} = \pi L\gamma_L \begin{pmatrix} z_c^{(t)} e_{31}^{(t)}(\mathrm{I}_L(kr_b) - \mathrm{I}_L(kr_a)) & z_c^{(b)} e_{31}^{(b)}(\mathrm{I}_L(kr_b) - \mathrm{I}_L(kr_a)) \\ z_c^{(t)} e_{31}^{(t)}(\mathrm{K}_L(kr_b) - \mathrm{K}_L(kr_a)) & z_c^{(b)} e_{31}^{(b)}(\mathrm{K}_L(kr_b) - \mathrm{K}_L(kr_a)) \\ L\alpha_1 z_c^{(t)} e_{31}^{(t)} \mathrm{J}_L^{\mathrm{I}}(r_b) & L\alpha_1 z_c^{(b)} e_{31}^{(b)} \mathrm{J}_L^{\mathrm{I}}(r_b) \\ L\alpha_1 z_c^{(t)} e_{31}^{(t)} \mathrm{Y}_L^{\mathrm{I}}(r_b) & L\alpha_1 z_c^{(b)} e_{31}^{(b)} \mathrm{Y}_L^{\mathrm{I}}(r_b) \\ L\alpha_2 z_c^{(t)} e_{31}^{(t)} \mathrm{I}_L^{\mathrm{I}}(r_b) & L\alpha_2 z_c^{(b)} e_{31}^{(b)} \mathrm{I}_L^{\mathrm{I}}(r_b) \\ L\alpha_2 z_c^{(t)} e_{31}^{(t)} \mathrm{K}_L^{\mathrm{I}}(r_b) & L\alpha_2 z_c^{(b)} e_{31}^{(b)} \mathrm{K}_L^{\mathrm{I}}(r_b) \end{pmatrix}, \tag{A.5b}$$

where the functions $\mathrm{J}_L^{\mathrm{I}}(r)$, $\mathrm{Y}_L^{\mathrm{I}}(r)$, $\mathrm{I}_L^{\mathrm{I}}(r)$, and $\mathrm{K}_L^{\mathrm{I}}(r)$ are defined in Eq. (32). The matrices $\mathbf{C}$, $\mathbf{G}_P$, and $\mathbf{P}_P$ of Eq. (41c) are as follows:

$$\mathbf{C} = \begin{pmatrix} C^{(t)} & 0 \\ 0 & C^{(b)} \end{pmatrix}, \tag{A.6a}$$

$$\mathbf{G}_p = \gamma_L \begin{pmatrix} 0 & 0 \\ 0 & 0 \\ 0 & 0 \\ e_{31}^{(t)} z_c^{(t)} \xi_1(r_b) & e_{31}^{(b)} z_c^{(b)} \xi_1(r_b) \\ e_{31}^{(t)} z_c^{(t)} \xi_2(r_b) & e_{31}^{(b)} z_c^{(b)} \xi_2(r_b) \\ e_{31}^{(t)} z_c^{(t)} \xi_3(r_b) & e_{31}^{(t)} z_c^{(t)} \xi_3(r_b) \end{pmatrix}, \tag{A.6b}$$

$$\mathbf{P}_p = \pi \gamma_L L^2 \zeta(r_b) \begin{pmatrix} z_c^{(t)2} e_{31}^{(t)2} & z_c^{(t)} z_c^{(b)} e_{31}^{(t)} e_{31}^{(b)} \\ z_c^{(t)} z_c^{(b)} e_{31}^{(t)} e_{31}^{(b)} & z_c^{(b)2} e_{31}^{(b)2} \end{pmatrix}, \tag{A.6c}$$

where $C^{(p)}$ is the clamped capacitance of the piezoelectric layer and defined as Eq. (19). The functions $\xi_i(r)$, $\zeta(r)$ are defined as

$$\xi_1(r) = \frac{\pi \alpha_1 L^2}{2D_{11}(\lambda_1^2 + \lambda_2^2)} (\mathrm{J}_L^D(\lambda_1 r)\mathrm{Y}_L^I(r) - \mathrm{Y}_L^D(\lambda_1 r)\mathrm{J}_L^I(r)) + \frac{\alpha_2 L^2}{D_{11}(\lambda_1^2 + \lambda_2^2)} (\mathrm{I}_L^D(\lambda_2 r)\mathrm{K}_L^I(r) - \mathrm{K}_L^D(\lambda_2 r)\mathrm{I}_L^I(r)), \tag{A.7a}$$

$$\xi_2(r) = \frac{-\pi \alpha_1 L^3}{2D_{11}(\lambda_1^2 + \lambda_2^2) r} (\mathrm{J}_L(\lambda_1 r)\mathrm{Y}_L^{\mathrm{I}}(r) - \mathrm{Y}_L(\lambda_1 r)\mathrm{J}_L^I(r)) - \frac{\alpha_2 L^3}{D_{11}(\lambda_1^2 + \lambda_2^2) r} (\mathrm{I}_L(\lambda_2 r)\mathrm{K}_L^{\mathrm{I}}(r) - \mathrm{K}_L(\lambda_2 r)\mathrm{I}_L^I(r)) - \frac{L \gamma_L}{r(G_{44} - \rho_R \omega^2)}, \tag{A.7b}$$

$$\xi_3(r) = \frac{\pi L^2}{2D_{11}(\lambda_1^2 + \lambda_2^2)} (\mathrm{J}_L(\lambda_1 r)\mathrm{Y}_L^I(r) - \mathrm{Y}_L(\lambda_1 r)\mathrm{J}_L^I(r)) + \frac{L^2}{D_{11}(\lambda_1^2 + \lambda_2^2)} (\mathrm{I}_L(\lambda_2 r)\mathrm{K}_L^I(r) - \mathrm{K}_L(\lambda_2 r)\mathrm{I}_L^I(r)), \tag{A.7c}$$

$$\zeta(r) = \frac{\pi \alpha_1 L^2}{2D_{11}(\lambda_1^2 + \lambda_2^2)} \int_{r_a}^{r} (\mathrm{J}_L(\lambda_1 r)\mathrm{Y}_L^I(r_b) - \mathrm{Y}_L(\lambda_1 r)\mathrm{J}_L^I(r_b))\,\mathrm{d}r + \frac{\alpha_2 L^2}{D_{11}(\lambda_1^2 + \lambda_2^2)} \int_{r_a}^{r} (\mathrm{I}_L(\lambda_2 r)\mathrm{K}_L^I(r_b) - \mathrm{K}_L(\lambda_2 r)\mathrm{I}_L^I(r_b))\,\mathrm{d}r + \frac{L^2 \gamma_L}{(\lambda_1^2 + \lambda_2^2)(G_{44} - \rho_R \omega^2)} \ln\left(\frac{r}{r_a}\right). \tag{A.7d}$$

References

[1] S. Ueha, Y. Tomikawa, Ultrasonic Motors, Theory and Applications, Science Publications, Oxford, 1993.
[2] K. Uchino, Piezoelectric Actuator and Ultrasonic Motors, Kluwer Academic Publisher, Boston, MA, 1996.

[3] M. Kurosawa, S. Ueha, Research and development of ultrasonic motor, Journal of the Acoustical Society of Japan 52 (1996) 910–914.
[4] I. Okumura, H. Mukohjima, A structure of ultrasonic motor for autofocus lenses, Proceeding of the Motor-Con'87, 1987, p. 75 .
[5] H. Das, X. Bao, Y. Bar-cohen, R. Bonitz, R. Lindemann, M. Maimone, I. Nesnas, C. Voorhees, Robot manipulator technologies for planetary exploration, Proceedings of the SPIE International Symposium on Smart Structures and Materials Conference, Newport Beach, CA, 1–5 March 1999, SPIE paper No. 3668-17.
[6] T. Sashida, Trial construction of ultrasonic motor, Oyo-Butsuri 51 (1982) 713–720.
[7] T. Yamabuchi, Y. Kagawa, Numerical simulation of a piezoelectric ultrasonic motor and its characteristics, Journal of the Japan Society of Simulation Technology (SIMULATION) 8 (1989) 69–76.
[8] T. Maeno, T. Tsukimoto, A. Miyake, Finite-element analysis of the rotor/stator contact in a ring-type ultrasonic motor, IEEE Transactions on Ultrasonics Ferroelectrics and Frequency Control 39 (1992) 668–674.
[9] Y. Kagawa, T. Tsuchiya, T. Kataoka, Finite element simulation of dynamic response of piezoelectric actuators, Journal of Sound and Vibration 191 (1996) 519–538.
[10] P. Hagedorn, J. Wallaschek, Travelling wave ultrasonic motors, Part I: working principle and mathematical modelling of the stator, Journal of Sound and Vibration 155 (1993) 31–46.
[11] P. Hagedorn, J. Wallaschek, W. Konrad, Travelling wave ultrasonic motors, Part II: a numerical method for the flexural vibrations of the stator, Journal of Sound and Vibration 168 (1993) 115–122.
[12] N.W. Hagood, A.J. Mcfarland, Modeling of a piezoelectric rotary ultrasonic motor, IEEE Transactions on Ultrasonics Ferroelectrics and Frequency Control 42 (1995) 210–224.
[13] P. Hagedorn, T. Sattel, D. Speziari, J. Schmidt, G. Diana, The importance of rotor flexibility in ultrasonic traveling wave motors, Smart Materials and Structures 7 (1998) 352–368.
[14] J.R. Friend, D.S. Stutts, The dynamics of an annular piezoelectric motor stator, Journal of Sound and Vibration 204 (1997) 421–437.
[15] S. Hirose, M. Aoyagi, Y. Tomikawa, S. Takahashi, K. Uchino, High-power characteristics at antiresonance frequency of piezoelectric transducers, Proceedings of the Ultrasonic International, Vol. 1, 1995.
[16] K. Uchino, Material issues in design and performance of piezoelectric actuators: an overview, Acta Mater 18 (1998) 3745–3753.
[17] E.C. Pestel, F.A. Leckie, Matrix Methods in Elastomechanics,, McGraw-Hill, New York, 1963.
[18] D.D. Ebenezer, Three-port parameters and equivalent circuit of radially polarized piezoelectric ceramic cylinders of finite length, Journal of the Acoustical Society of America 99 (1996) 2908–2912.
[19] L. Shuyu, Equivalent circuits and directivity patterns of air-coupled ultrasonic transducers, Journal of the Acoustical Society of America 109 (2001) 949–957.
[20] R.D. Mindlin, Influence of rotatory inertia and shear on flexural motions of isotropic, elastic plates, Journal of Applied Mechanics 18 (1951) 31–38.
[21] R.D. Mindlin, H. Deresiewicz, Thickness-shear and flexural vibrations of a circular disk, Journal of Applied Physics 25 (1954) 1329–1332.
[22] S.K. Ha, Admittance matrix of asymmetric piezoelectric bimorph with two separate electrical ports under general distributed loads, IEEE Transactions on Ultrasonics Ferroelectrics and Frequency Control 48 (2001) 976–984.
[23] S. Sherrit,B.K. Mukherjee, The use of complex material constants to model the dynamic response of piezoelectric materials, Proceedings of the IEEE Ultrasonics Symposium, Vol. 1, 1998, pp. 633–640.
[24] S.K. Ha, Y.H. Kim, Impedance and admittance matrices of symmetrical piezoelectric annular bimorphs and their applications, Journal of the Acoustical Society of America 108 (2000) 2125–2133.
[25] Ansys, ANSYS User's Manual, Swanson Analysis Systems Inc., Houston, PA, 1995.
[26] D. Boucher, M. Lagier, C. Maerfeld, Computation of the vibrational modes for piezoelectric array transducer using a mixed finite element-perturbation method, IEEE Transactions on Sonics and Ultrasonics SU-28 (1981) 318–330.
[27] A. Iino, K. Suzuki, M. Kasuga, M. Suzuki, T. Yamanaka, Development of a self-oscillating ultrasonic micro-motor and its application to a watch, Ultrasonics 38 (2000) 54–59.